AIP | Applied Physics Letters

Spin-crossover molecule based thermoelectric junction

Dibyajyoti Ghosh, Prakash Parida, and Swapan K. Pati

Citation: Applied Physics Letters **106**, 193105 (2015); doi: 10.1063/1.4921165
View online: http://dx.doi.org/10.1063/1.4921165
View Table of Contents: http://scitation.aip.org/content/aip/journal/apl/106/19?ver=pdfcov
Published by the AIP Publishing

Spin-crossover molecule based thermoelectric junction

Dibyajyoti Ghosh,[1] Prakash Parida,[2] and Swapan K. Pati[3]
[1]*Chemistry and Physics of Materials Unit, Jawaharlal Nehru Centre for Advanced Scientific Research, Bangalore 560064, India*
[2]*Institute for Theoretical Physics, University of Regensburg, D-93040 Regensburg, Germany*
[3]*Theoretical Sciences Unit, Jawaharlal Nehru Centre for Advanced Scientific Research, Bangalore 560064, India*

(Received 29 September 2014; accepted 2 May 2015; published online 13 May 2015)

Using *ab-initio* numerical methods, we explore the spin-dependent transport and thermoelectric properties of a spin-crossover molecule (i.e., iron complex of 2-(1H-pyrazol-1-yl)-6-(1H-tetrazole-5-yl)pyridine) based nano-junction. We demonstrate a large magnetoresistance, efficient conductance-switching, and spin-filter activity in this molecule-based two-terminal device. The spin-crossover process also modulates the thermoelectric entities. It can efficiently switch the magnitude as well as spin-polarization of the thermocurrent. We find that thermocurrent is changed by ~4 orders of magnitude upon spin-crossover. Moreover, it also substantially affects the thermopower and consequently, the device shows extremely efficient spin-crossover magnetothermopower generation. Furthermore, by tuning the chemical potential of electrodes into a certain range, a pure spin-thermopower can be achieved for the high-spin state. Finally, the reasonably large values of figure-of-merit in the presence and absence of phonon demonstrate a large heat-to-voltage conversion efficiency of the device. We believe that our study will pave an alternative way of tuning the transport and thermoelectric properties through the spin-crossover process and can have potential applications in generation of spin-dependent current, information storage, and processing. © *2015 AIP Publishing LLC*. [http://dx.doi.org/10.1063/1.4921165]

Recent discovery of several fascinating properties like giant magnetoresistance,[1] spin-injection,[2] spin-filtration,[3–6] and negative differential resistance[7,8] has attracted huge research interest in the field of molecular spintronics.[9–11] Contemporarily, these molecular devices are hugely explored for their promising thermoelectric effects, i.e., ability of converting heat to electrical power.[12,13] Furthermore, successful coupling of spintronics and thermoelectricity has introduced another promising research-field, spin-caloritronics.[14,15]

Although single molecular-magnets could be a good choice for molecular spintronics, several disadvantages like ultralow critical-temperature and poor structural stability limit their usage.[16,17] However, the usage of magnetically bistable, spin-crossover (SCO) molecules would be another promising way to tune the spin-states.[18–20] Recent studies demonstrating the SCO phenomenon in single molecular level also support the possibility to realize single molecular switching devices in recent future.[20–22] Apart from the ground state, these molecules have one or more metastable magnetic states which can be accessible by applying different external stimuli.[23] Generally, these molecules contain first-row transition-metal (TM) atom(s) with electronic configuration, $3d^4$–$3d^7$ as the spin center(s).[23] However, low transition temperature of temperature-induced SCO molecules, which are mostly explored in literature, restrict their usage as room-temperature switching devices.[23] Interestingly, Schafer *et al.* have recently synthesized a neutral iron complex using 2-(1H-pyrazol-1-yl)-6-(1H-tetrazole-5-yl)pyridine (LH) ligand which shows a sharp transition from the low-spin (LS, $S = 0$) state to high-spin (HS, $S = 2$) state at room temperature.[24] To explore the conductance-switching and magnetoresistance properties of this SCO molecule, in this letter we perform the state-of-art density functional theory (DFT) combining with non-equilibrium Greens function (NEGF) based electron transport calculations. Furthermore, we report an extraordinary thermoelectric efficiency of this molecular junction.

As relative stability between LS and HS states of the SCO-molecule highly depends on the choice of different exchange-correlation functionals,[25] we optimize the isolated molecule using various exchange-correlation functionals to find the appropriate functionals. We use General Gradient Approximation and three hybrid functionals with different amount/types of Hartree-Fock (HF) exchange-interactions, i.e., Becke three-parameter Lee-Yang-Parr hybrid (i.e., B3LYP) (20% HF exchange),[26,27] PBE0 (25% HF exchange),[28] and HSE06 (25% short-range HF exchange)[29] as implemented in Gaussian 09.[30] Without imposing any symmetry constraints during optimization, we find the stable molecular conformations in the LS and HS states, separately. As shown in Fig. 1(a), Fe atom, which stays at the center of a slightly distorted octahedron, gets surrounded by two identical tridentate ligands, 2-(pyrazol-1-yl)-6-(tetrazol-1-yl) pyridine. Like previous reports,[25] spin-crossover from LS to HS prominently elongates Fe-N bonds by 0.10–0.28 Å due to the electron rearrangement in e_g orbitals (i.e., $d_{x^2-y^2}/d_{z^2}$) of Fe. Notably, none of the hybrid functionals (i.e., B3LYP, PBE0, and HSE06) is able to determine the ground state spin-configuration accurately for the present molecule. As these hybrid functionals overestimate the exchange energy, they incorrectly stabilize the HS state of the SCO molecule.[25] Only GGA functionals predict LS as the ground state where the energy gap between LS and HS states is 1.51 eV. Furthermore, within GGA functionals, the optimized molecule in its LS state shows excellent agreement with available experimental crystal data.[24] Thus, we choose this

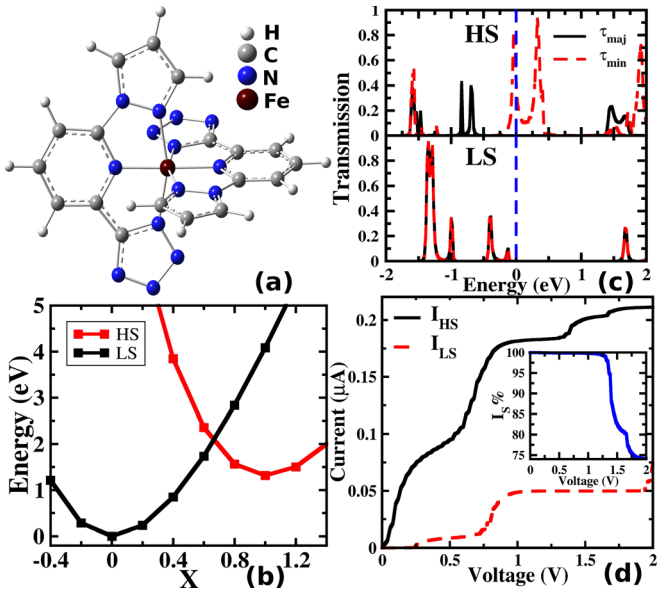

FIG. 1. (a) The molecular structure of Fe(2-(1H-pyrazol-1-yl)-6-(1H-tetrazole-5-yl)pyridine)$_2$ ([Fe(L)$_2$]). (b) Energy E for HS and LS states along X. Energies are scaled to E at X = 0. (c) Zero-bias spin-polarized transmission spectra for HS (upper panel) and LS (lower panel) states as a function of energy. (d) I—V characteristics for HS and LS states. I_S—V plot is shown in the inset.

functionals for further investigations. Note that close structural match between isolated molecule and its crystallographic data also signifies that these molecules remain weakly packed due to intermolecular π-π stacking in their crystalline form.

In Fig. 1(b), we plot the total energy as a function of reaction coordinate, X. Here, X is varied from X = 0 (LS state) to X = 1 (HS state). The LS state at X = 0 appears much more stable than that of HS state at X = 1, demonstrating the LS state as the ground state at 0 K. At X = 0.66 where the LS and HS states become almost degenerate in energy, molecular spin-crossover occurs from LS to HS.

Now, we briefly explore the spin-dependent electron transmission of the SCO molecule-based nano-device. This molecule gets sandwiched between two (111) plane of gold electrodes through sulfur ligands on either side. This two-terminal device is named as electrode-molecule-electrode (E-M-E) system. Using SIESTA package,[31] we optimized the geometry of E-M-E system. To calculate transmission spectra, we have used NEGF methodology extended for spin-polarized systems as implemented in TranSIESTA package.[32] Note that as the previous studies suggested that transmission function of SCO-based molecular-junctions has insignificant effects over electrode-molecule contact-geometries, we exclude other energetically less stable contact-structures.[19,20]

Although previous studies have shown the instability of similar molecules upon deposition to electrode-surfaces,[16] [Fe(L)$_2$] almost retains its molecular structure even after adsorption onto the gold electrodes. Most importantly, after deposition, LS-HS energy separation of this molecule becomes 1.22 eV, which is slightly lesser than its gas-phase value. As this large energy-gap cannot be closed by environmental influences, we conclude that [Fe(L)$_2$] can exhibit sharp spin-state switching in the modeled molecular device. Importantly, experimental study using X-ray absorption spectroscopy has already demonstrated temperature induced sharp LS-HS transition for single SCO molecules on Au(111) surface.[21]

In Fig. 1(c), we explore the spin polarized zero-bias transmission coefficient τ(E) for both the spin states within the energy window of −2 eV to 2 eV. Using Landauer–Büttiker formalism,[33] total conductance (G) at Fermi energy (E_F) can be formulated as $G = (\frac{e^2}{h})\sum_\sigma \tau_\sigma(E_F)$, where $\tau_\sigma(E_F)$ is the transmission coefficient for the spin channel σ at E_F. As resonant transmission peaks near to E_F change quite distinctly with the molecular phase-transition from LS to HS, we consequently find a substantial increment in G. We can quantify the change in G by calculating the magnetoresistance ratio, defined as $\frac{(G_{HS}-G_{LS})}{(G_{HS}+G_{LS})}$. Interestingly, the calculated zero-bias magnetoresistance turns out to be ∼100% at E_F which shows a sharp conductance switching of this device upon spin-crossover. We note that the electrical conductance through [Fe(L)$_2$] can be switched on/off simply by tuning the molecular spin states in the spin-crossover process.

As can be seen from Fig. 1(c), for HS state, at and near the E_F, minority-spins show prominent transmission peaks, whereas majority-spins open up a transport gap of 2.1 eV. Thus, under a finite bias, the device can exhibit extremely efficient spin-filter activity. We define spin polarization of transmission ($\tau_{S(HS/LS)}$) for a particular spin state as[3]

$$\tau_{S,HS/LS} = \frac{|\tau_{min}(E_F) - \tau_{maj}(E_F)|}{\tau_{min}(E_F) + \tau_{maj}(E_F)}, \quad (1)$$

where τ_{min} (τ_{maj}) is the transmission coefficient for the minority-spin (majority-spin) channel. As transmission spectra are completely spin-unpolarized and ∼100% spin-polarized for LS and HS states, respectively, τ_S changes sharply from 0% to ∼100% upon spin-crossover. The rearrangement of electrons in 3d orbitals of Fe during LS to HS transition abruptly changes the position of transport-active channels near E_F, resulting in a sharp modification of zero-bias transmission coefficient. Importantly, for HS state, only minority-spin molecular orbitals strongly couple with the electrode-states at and near E_F, resulting in ∼100% spin-polarization of transmission at that energy.

As real-world-devices work at a finite bias, we plot the current (I)–source-drain voltage (V_{SD}) characteristics in Fig. 1(d). Here, the total-current is calculated by Landauer–Büttiker formula[33]

$$I_{HS/LS} = \left(\frac{e}{h}\right)\sum_\sigma \int_{\mu_L}^{\mu_R} \tau_{\sigma,HS/LS}(E, V_{SD})dE. \quad (2)$$

For V ≤ 0.2 V, the I_{HS}/I_{LS} ratio reaches up to ∼700, which is quite high. Such a huge modification of current at low bias during the spin-crossover exhibits the SCO-mediated switching behavior. To demonstrate the spin-filter property of HS state, we compute the spin resolved I—V_{SD} where the minority-spin current reaches ∼0.2 μA, while the majority-spin component remains almost zero. To quantify this, we calculate spin-resolved current (I_S) at a particular voltage, V, as[3]

$$I_S = \frac{|I_{min}(V) - I_{maj}(V)|}{(I_{min}(V) + I_{maj}(V))}, \quad (3)$$

where $I_{min(maj)}(V)$ denotes minority (majority) current. It can be evidently seen that I_S remains ~100% up to 1.2 V and then reduces as the bias increases further (inset of Fig. 1(d)).

Simultaneous measurements of conductance and thermoelectric properties in E-M-E systems motivate us to discuss spin-dependent thermoelectric effects of the present nanojunction.[13,34] The thermocurrent induced by temperature-difference in two electrodes is calculated by using Landauer formula.[35] The temperature difference is denoted as $T_{SD} = |T_S - T_D|$, where T_S (T_D) is temperature of source (drain) electrode. The thermocurrent reads as

$$I_{thermo,\sigma} = \frac{e}{h}\int \tau_\sigma(E)[f_S(T_S, E) - f_D(T_D, E)]dE, \quad (4)$$

where f_S (f_D) is the Fermi distribution function for source (drain). In the linear response regime, we formulate spin-resolved Seebeck coefficient, $S_\sigma = \frac{1}{eT}\frac{L_{1,\sigma}(T,\mu)}{L_{0,\sigma}(T,\mu)}$, where $L_{n,\sigma}(T,\mu) = \frac{1}{h}\int \tau_\sigma(E)(E-\mu)^n[-\partial_E f(E,\mu,T)]dE$ (n = 0, 1, 2), T is temperature of the whole system, and μ is chemical potential of electrodes.[36] To calculate the charge-Seebeck coefficient (S_C), we use the total transmission, i.e., $\tau_{tot} = \sum_\alpha \tau_\alpha$, whereas the spin-polarized Seebeck (S_S) is formulated as $S_S = (S_{maj} - S_{min})$, where $S_{maj(min)}$ is majority (minority)-spin Seebeck-coefficient.[37] Further, we define the figure-of-merit as $ZT = \frac{S_C G T}{\kappa_e + \kappa_{ph}}$, where G is the charge conductance (i.e., $G = |L_{0,maj} + L_{0,min}|$ and $\kappa_{e(ph)}$ is the electronic (phonon) thermal conductance (i.e., $\kappa_e = \frac{1}{T}\left(L_2 - \frac{L_1^2}{L_0}\right)$).[38] Importantly, as several studies have proposed different ways to suppress the κ_{ph} to the thermopower in molecular junctions,[39–43] first we calculate $Z^{el}T$ neglecting this term. However, later on, we also calculate thermoelectric figure-of-merit, i.e., ZT, including phonon contribution. Note that as molecular spin-crossover temperature is ≈295 K,[24] we consider the molecule with LS (HS) state when the average molecular temperature (i.e., $T_{mol} = (T_S + T_D)/2$) remains ≤295 K (>295 K).

We now calculate the thermally induced current ($I_{thermo,HS/LS}$) for both spin-states as a function of T_S at different T_{SD}. Note that as maximum $T_{SD} = 100$ K, molecule can retain LS state up to $T_S \leq 345$ K, above which it transforms to HS state. Figs. 2(a) and 2(b) show that $I_{thermo,HS}$ is several times higher than $I_{thermo,LS}$. Below a certain threshold T_S (T_{th}), i.e., ~160–280 K (depending on T_{SD}), $I_{thermo,LS} \approx 0$. Consequently, as shown in Fig. 2(c), at $T_S \approx 345$ K and $T_{SD} = 100$ K (i.e., at T_C), thermocurrent can increase by ~4 orders of magnitude upon spin-crossover. Moreover, the I_{on}/I_{off} ratio of I_{thermo} also reaches maximum of 10^{13} (Fig. 2(c)). These results demonstrate the molecular junction as a high-performance-switching device. In fact, when $T_{SD} > 0$, it makes $[f_S(T_S, E) - f_D(T_D, E)] \neq 0$ and thermocurrent flows only if $\tau_{maj/min}(E)$ is finite at the applied temperature-difference window. Moreover, I_{thermo} is proportional to the area under the active transmission spectra. Now, as only HS state has finite transmission probability at and around E_F,

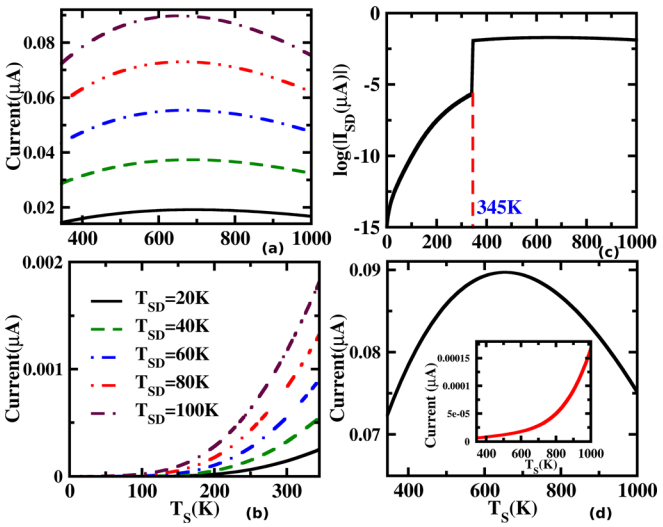

FIG. 2. I_{thermo} verses T_S with various T_{SD} for (a) HS and (b) LS states; (c) $\log(I_{SD})$ verses T_S plot with $T_{SD} = 100$ K; and (d) minority-spin current for HS state verses T_S with $T_{SD} = 100$ K. The corresponding majority-spin current is shown in the inset.

$I_{thermo,HS}$ is much larger than $I_{thermo,LS}$ at *spin-crossover temperature* and moderate T_{SD}. Additionally, for LS state, T_S needs to cross T_{th} to switch-on thermo-transport by activating the closest transmission peak (i.e., at −0.12 eV).

Focusing on spin-polarized thermocurrent at HS state, as only τ_{min} is finite at and around E_F (Fig. 1(c)), applying a very small temperature-difference we can obtain 100% spin-polarized carrier transport through the molecular junction (see Fig. 2(d) and the inset of it). Thus, the junction acts as a pure spin-polarized current generator. On the other hand, as the transmission function is spin-independent for LS state, thermocurrent becomes spin unpolarized here. Thus, controlling the temperature of system, we can efficiently switch on/off the spin polarization of the thermocurrent.

From Figs. 2(a) and 2(b), we note that (1) for both the spin-states, the I_{thermo} increases with T_{SD}. Essentially, as T_{SD} increases, more carriers become transport active, resulting in a rise in the total current. (2) $I_{thermo,HS}$ reaches its maxima at $T_S \approx 650$ K–700 K and then decreases at higher T_S. In fact, at smaller T_S, minority-spin holes mostly carry the current, whereas electron-mediated current becomes significant at higher T_S and as stated later, it counteracts with the hole-current. Thus, the total $I_{thermo,HS}$ gets reduced for $T_S > 650$ K–700 K. For LS state, as only hole-current gets generated within the temperature range of $0 \leq T_S \leq 345$ K, $I_{thermo,LS}$ keeps on increasing with T_S (Fig. 2(b)).

Next, we investigate the relation between S_σ and chemical potential (μ) of the electrodes. As $V_{SD} = 0$, the chemical potential of electrodes (i.e., μ_L, μ_R) is equal to the equilibrium E_F. Within linear response regime, we assume $T_S \approx T_D = 350$ K (250 K) for HS (LS) state and vary μ as $-1 \leq \mu \leq 1$. As the spin-dependent transmission spectra strongly influence the thermopower generation, this device exhibits an abrupt change in S_C and S_S during spin-crossover of the molecule (see Fig. 3(a)). Note that as electrons and holes (i.e., active carriers for heat-conduction) move in opposite directions to each other, one must break electron-hole symmetry to achieve non-zero thermopower at a particular μ. In other words, G(E)

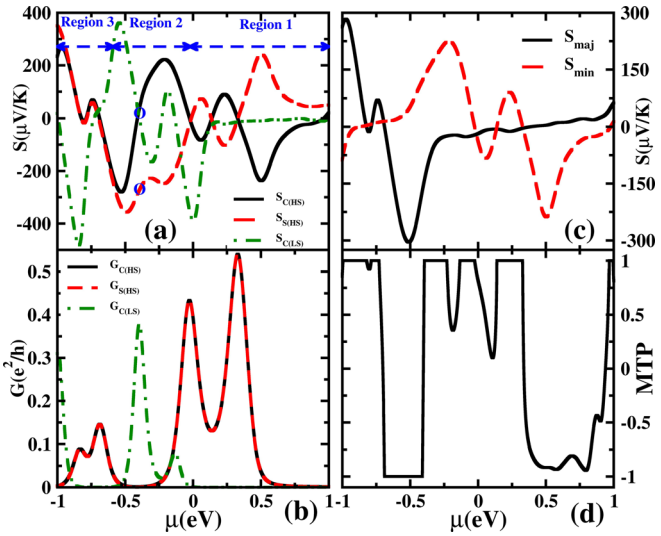

FIG. 3. (a) $S_{C(HS)}$, $S_{S(HS)}$, and $S_{C(LS)}$ and (b) $G_{C(HS)}$, $G_{S(HS)}$, and $G_{C(LS)}$ as a function of μ. Three distinct regions in (a) are separated by blue arrows. At $\mu \approx -0.41$ eV, values of S_C and S_S are pointed by blue circles. We consider $T_S \approx T_D = 350$ K (250 K) for HS (LS) state. (c) S_{maj}, S_{min} and (d) MPT for HS state as a function of μ.

around μ must be asymmetric in nature. By tuning μ, i.e., shifting the position of E_F, we eventually modify the carrier-types (i.e., electrons or holes). Note that if electrons (holes) are the dominant carriers at E_F, thermopower becomes negative (positive). From Figs. 3(a)–3(c), we find that (1) wherever G(E) is negligible or shows peak, thermopower is almost zero due to the presence of electron-hole symmetry and (2) S shows a finite value when finite conductance and electron-hole asymmetry appear simultaneously. Moreover, we also find a sign-change of thermopower wherever conductance peaks appear. This occurrence is due to the fact that the carrier-type changes sign as μ crosses the peak position. As an example, at $\mu = 0$, S_C of HS state ($S_{C(HS)}$) is -38 μV/K as electrons are the dominant thermopower-carrier (see Fig. 3(a)). However, at $\mu = -0.027$ eV, E_F reaches the peak of $G_{C(HS)}(E)$ where the electron-hole symmetry appears, resulting in $S_{C(HS)} \approx 0$ (see Figs. 3(a) and 3(b)). As we move to higher negative μ value, electron-hole symmetry breaks down and holes become the dominant thermopower-carrier, making the $S_{C(HS)} > 0$. Notably, $S_{C(HS)}$ reaches the maximum value of 222 μV/K at $\mu = -0.21$ eV where only holes are the active carriers. At more negative μ, electrons start contributing again, resulting in the reduction of $S_{C(HS)}$. (3) For the LS state, as τ_{maj} and τ_{min} are identical, the G and thermopower (S_{LS}) are completely spin-independent. Interestingly, the charge Seebeck coefficient for low-spin state, $S_{C(LS)}$, reaches a high value of -484 μV/K at $\mu = -0.84$ eV due to sharp peak in the conductance (see Figs. 3(a) and 3(b)).

Furthermore, Figs. 3(a) and 3(c) evidently show that one can control the magnitude and direction of charge and spin-thermopower to a great extent. In Figs. 3(a) and 3(c), we find three distinct regions for HS state (shown by blue arrows in Fig. 3(a)), (1) -0.02 eV $< \mu < 1$ eV where $S_C \approx -S_S$ and minority-spin electrons carry the thermopower; (2) -0.59 eV $< \mu < -0.02$ eV, where $S_C < S_S$ and both spin channels are active; and (3) -1 eV $< \mu < -0.59$ eV, where $S_C \approx S_S$ and only majority-spin carry thermopower. The second region is most important as S_S greatly exceeds S_C. In this region, thermopower carried by majority-spin electrons and minority-spin holes moves in opposite direction and gets collected in different electrodes. It results in S_C to be small in magnitude, while S_S becomes quite large. Particularly at $\mu \approx -0.41$ eV where $S_C = 0$ but $S_S = -289$ μV/K (see the blue circles in Fig. 3(a)), we could achieve pure spin-thermopower without any charge component. For the LS state, as S_{LS} is spin-independent, we find $S_C = S_{LS}$ and $S_S = 0$. As the thermopower gets modified remarkably with the spin-crossover, we quantify this change by defining magnetothermopower (MPT)[44] as $\frac{S_{C(HS)} - S_{C(LS)}}{S_{C(HS)} + S_{C(LS)}}$ which is plotted in Fig. 3(d). We find that magnetothermopower is $\approx \pm 1$ which explicitly demonstrates the ability to tune the thermopower generation by controlling the spin-state of the molecule.

Finally, we investigate the efficiency of this molecular junction towards thermoelectric conversion. Here, figure-of-merit shows an oscillating behavior as conductance and thermopower are inversely correlated.[45] Considering $\kappa_{ph} = 0$, tuning the μ to -0.91 eV at HS state results in the highest value of 4.65 for $Z^{el}T$ (Fig. 4(a)). At LS state, we find highest $Z^{el}T$ as 20, which is quite higher than HS state (see Fig. 4(b)).

Now, to include the phonon contribution to the thermal conductance, we use the equation $\kappa_{ph} = 3\kappa_0$, where $\kappa_0 = \pi^2 k_B{}^2 T/3h$, i.e., the quantum of thermal conductance.[38,46] The position of peaks of ZT does not change even after inclusion of κ_{ph} (see Figs. 4(c) and 4(d)). However, the relative magnitude of them gets modified largely for both the spin states. Importantly, the absolute magnitude of ZT gets reduced due to phonon mediated thermal conductance.

Following the work by Chapuis *et al.*, we find that the heat transfer due to near-field radiation is $\approx 10^{3.5}$ W m^{-2} K^{-1} for our system.[47] This quantity is quite negligible compared to the electronic heat transfer through molecular junction ($\approx 10^6$ (10^4) W m^{-2} K^{-1} for HS (LS) states). Thus, we can neglect the contribution of near-field radiative heat transfer for the present study.

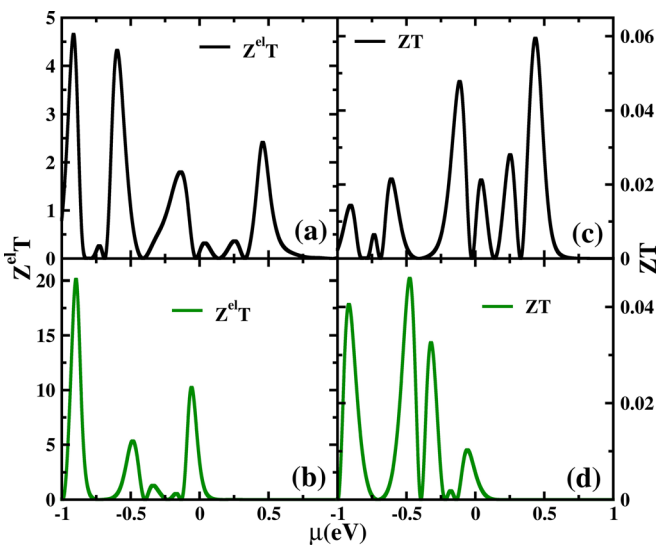

FIG. 4. $Z^{el}T$ for (a) HS and (b) LS states; ZT for (c) HS and (d) LS states. We consider $T_S \approx T_D = 350$ K (250 K) for HS (LS) state. Note that the position of peaks does not change with inclusion of phonon contribution. But relative peak-values do change.

In conclusion, we have discussed configurational changes and stability of different spin states during spin-crossover process. Upon spin-crossover, we surmise a huge modulation in electronic and thermoelectric entities. The theoretical prediction of extraordinary efficiency of conductance-switching, spin-filter, magnetoresistance, and heat-to-voltage conversion of this SCO molecule based junction will certainly make our study more impact in the field of spin caloritronics.

S.K.P. acknowledges research support from the CSIR and DST, Government of India.

[1]Z. H. Xiong, D. Wu, Z. V. Vardeny, and J. Shi, Nature **427**, 821 (2004).
[2]A. J. Drew, J. Hoppler, L. Schulz, F. L. Pratt, P. Desai, P. Shakya, T. Kreouzis, W. P. Gillin, A. Suter, N. A. Morley *et al.*, Nat. Mater. **8**, 109 (2009).
[3]P. Parida, E. A. Basheer, and S. K. Pati, J. Mater. Chem. **22**, 14916 (2012).
[4]S. Sanvito, Nat. Mater. **10**, 484 (2011).
[5]P. Parida, A. Kundu, and S. K. Pati, Phys. Chem. Chem. Phys. **12**, 6924 (2010).
[6]D. Ghosh, P. Parida, and S. K. Pati, J. Phys. Chem. C **116**, 18487 (2012).
[7]P. Parida, S. Lakshmi, and S. K. Pati, J. Phys.: Condens. Matter **21**, 095301 (2009).
[8]P. Parida, S. K. Pati, and A. Painelli, Phys. Rev. B **83**, 165404 (2011).
[9]S. Sanvito and A. R. Rocha, J. Comput. Theor. Nanosci. **3**(5), 624 (2006).
[10]S. Sanvito, Nat. Phys. **6**, 562 (2010).
[11]S. Sanvito, Chem. Soc. Rev. **40**, 3336 (2011).
[12]Y. Dubi and M. Di Ventra, Rev. Mod. Phys. **83**, 131 (2011).
[13]J. R. Widawsky, P. Darancet, J. B. Neaton, and L. Venkataraman, Nano Lett. **12**, 354 (2012).
[14]G. E. W. Bauer, E. Saitoh, and B. J. van Wees, Nat. Mater. **11**, 391 (2012).
[15]K. Uchida, S. Takahashi, K. Harii, J. Ieda, W. Koshibae, K. Ando, S. Maekawa, and E. Saitoh, Nature **455**, 778 (2008).
[16]M. Mannini, P. Sainctavit, R. Sessoli, C. Cartier dit Moulin, F. Pineider, M. A. Arrio, A. Cornia, and D. Gatteschi, Chem. - Eur. J. **14**, 7530 (2008).
[17]M. Urdampilleta, S. Klyatskaya, J. P. Cleuziou, M. Ruben, and W. Wernsdorfer, Nat. Mater. **10**, 502 (2011).
[18]T. Miyamachi, M. Gruber, V. Davesne, M. Bowen, S. Boukari, L. Joly, F. Scheurer, G. Rogez, T. K. Yamada, P. Ohresser *et al.*, Nat. Commun. **3**, 938 (2012).
[19]N. Baadji and S. Sanvito, Phys. Rev. Lett. **108**, 217201 (2012).
[20]D. Aravena and E. Ruiz, J. Am. Chem. Soc. **134**, 777 (2012).
[21]B. Warner, J. C. Oberg, T. G. Gill, F. El Hallak, C. F. Hirjibehedin, M. Serri, S. Heutz, M.-A. Arrio, P. Sainctavit, M. Mannini *et al.*, J. Phys. Chem. Lett. **4**, 1546 (2013).
[22]M. Bernien, D. Wiedemann, C. F. Hermanns, A. Krüger, D. Rolf, W. Kroener, P. Müller, A. Grohmann, and W. Kuch, J. Phys. Chem. Lett. **3**, 3431 (2012).
[23]P. Gütlich and H. A. Goodwin, *Spin Crossover in Transition Metal Compounds* (Springer, New York, 2004).
[24]B. Schafer, C. Rajnak, I. Salitros, O. Fuhr, D. Klar, C. Schmitz-Antoniak, E. Weschke, H. Wende, and M. Ruben, Chem. Commun. **49**, 10986 (2013).
[25]A. Droghetti, D. Alfè, and S. Sanvito, J. Chem. Phys. **137**, 124303 (2012).
[26]A. D. Becke, J. Chem. Phys. **98**, 5648 (1993).
[27]C. Lee, W. Yang, and R. G. Parr, Phys. Rev. B **37**, 785 (1988).
[28]C. Adamo and V. Barone, J. Chem. Phys. **110**, 6158 (1999).
[29]J. Heyd, G. E. Scuseria, and M. Ernzerhof, J. Chem. Phys. **118**, 8207 (2003).
[30]M. J. Frisch, G. W. Trucks, H. B. Schlegel, G. E. Scuseria, M. A. Robb, J. R. Cheeseman, G. Scalmani, V. Barone, B. Mennucci, G. A. Petersson *et al.*, in Gaussian 09 (2009).
[31]J. M. Soler, E. Artacho, J. D. Gale, A. Garcia, J. Junquera, P. Ordejon, and D. Sanchez-Portal, J. Phys.: Condens. Matter **14**, 2745 (2002).
[32]M. Brandbyge, J. L. Mozos, P. Ordejon, J. Taylor, and K. Stokbro, Phys. Rev. B **65**, 165401 (2002).
[33]S. Datta, *Electronic Transport in Mesoscopic Systems* (Cambridge University Press, Cambridge, England, 1995).
[34]S. Guo, G. Zhou, and N. Tao, Nano Lett. **13**, 4326 (2013).
[35]M. Zeng, Y. Feng, and G. Liang, Nano Lett. **11**, 1369 (2011).
[36]Y. S. Liu, X. F. Yang, F. Chi, M. S. Si, and Y. Guo, Appl. Phys. Lett. **101**, 213109 (2012).
[37]M. Czerner, M. Bachmann, and C. Heiliger, Phys. Rev. B **83**, 132405 (2011).
[38]Y. Dubi and M. Di Ventra, Phys. Rev. B **79**, 081302 (2009).
[39]H. Nakamura, T. Ohto, T. Ishida, and Y. Asai, J. Am. Chem. Soc. **135**, 16545 (2013).
[40]Y. Asai, Phys. Rev. B **84**, 085436 (2011).
[41]C. Finch, V. García-Suárez, and C. Lambert, Phys. Rev. B **79**, 033405 (2009).
[42]J. P. Bergfield, M. A. Solis, and C. A. Stafford, ACS Nano **4**, 5314 (2010).
[43]Y. Liu, Y. Chen, and Y. Chen, ACS Nano **3**, 3497 (2009).
[44]K. Zberecki, M. Wierzbicki, J. Barnaś, and R. Swirkowicz, Phys. Rev. B **88**, 115404 (2013).
[45]M. Zeng, W. Huang, and G. Liang, Nanoscale **5**, 200 (2013).
[46]D. Segal, A. Nitzan, and P. Hänggi, J. Chem. Phys. **119**, 6840 (2003).
[47]P. Chapuis, S. Volz, C. Henkel, K. Joulain, and J. Greffet, Phys. Rev. B **77**, 035431 (2008).